Hyperspectral Anomaly Detection Using Outlier Removal from Collaborative Representation

Maryam Vafadar
Department of Electrical Engineering,
Science and Research Branch,
Islamic Azad University
Tehran, Iran
vafadar.mar@gmail.com

Hassan Ghassemian
Image Processing and Information Analysis Lab.
Faculty of Electrical and Computer Engineering
Tarbiat Modares University
Tehran, Iran
ghassemi@modares.ac.ir

Abstract—**Hyperspectral imagery systems have the ability to collect 3D digital images with rich spatial and spectral information. Anomaly detection is one of the interesting applications over last two decades in hyperspectral imagery. In this paper, we propose Collaborative Representation-Based with Outlier Removal Anomaly Detector (CRBORAD) method for HSI Anomaly Detection. We use both spectral and spatial information for detecting anomalies instead of using only spectral information that was introduced in our previous work. The proposed detector can adaptively estimate the background by its adjacent pixels within a sliding dual window. Before estimating background pixels, we remove outlier pixels that are significantly different from majority of pixels. It leads us to precise background approximation and better accuracy for detecting anomalies in subsequent stages. The residual image is constituted by subtracting the predicted background from the original HSI, and anomalies can be determined in the residual image, finally. Kernel extension of the proposed approach is also presented. We implemented the proposed algorithms on San Diego airport hyperspectral data. CRBORAD results are illustrated using receiver-operating-characteristic (ROC) curves, Area Under Curve (AUC) values and intuitive images. Comparing the results of the current study with four popular and previous methods shows that CRBORAD provides us an accurate method for detecting anomalies.**

Keywords-Hyperspectral imagery; Anomaly detection; collaborative representation; kernel collaborative representation; remote sensing; residual image

I. INTRODUCTION

Hyperspectral imagery systems provide 3D digital images in both spatial and spectral dimensions. Hyperspectral 3D images measure scientifically the received radiance at fine divided bands across a range of wavelengths. So sampled spectra for each pixel is obtained densely; it is an efficient tool for many successful applications [1-2]. Like environmental monitoring [3], production quality inspection, medical imaging, biological analysis [4-5], etc. The rich information about the spectral signatures of pixels can discriminate various materials. Target detection has been one of the most interesting and fundamental tasks in hyperspectral imagery [6].

Two types of target detection techniques are usually interested in target detection domain: known and unknown with target spectra. If target spectra are known in the processing of target detectors, detectors will require the spectral information about the targets of interest and it is also named spectral matching detection algorithms. These detectors try to match pixels with spectral information of targets. However, in most cases, it is difficult to obtain the spectrum of targets. The absorption and scattering of the atmosphere, the subtle effects of illumination and the spectral response of the sensor must all be considered in measuring the spectral properties of a material through the atmosphere. Moreover, spectral variability also needs to be addressed in this kind of target detection. So, in most cases the accurate spectrum signatures of many interesting signals or targets cannot be provided in advance.

Another target detection without target spectra is called anomaly detection. Anomaly detection algorithms are more practical in actual applications. This technique does not require any prior features or information of targets of interest. Anomaly detection has been of great interest in hyperspectral imagery processing in recent twenty years [7–8] and is applied to many application domains such as precision agriculture, rare mineral discovery in geology, civilian search and rescue, man-made objects distinction in intelligent defense and military purposes [9], border monitoring, etc. The goal of anomaly detection is to detect a small quantity of pixels in the hyperspectral image whose spectral characteristics differ significantly from those of a large proportion of pixels in the hyperspectral data cube, and then the hyperspectral image is segmented into two parts: anomaly targets and backgrounds. For example, with national defense, anomalies may be tanks, aircraft, launchers, and other objects of military significance scattered across a battle field. And for civilian applications, anomalies may be vehicles located in an urban or natural field.

Generally, the aim of Anomaly Detection in hyperspectral remote sensing is to locate a target whose distinct spectrum deviates significantly from the background [10]. A wealth of anomaly detection methods has been proposed over last two decades [11]. One of the conventional detectors is statistical methods. These methods need some rigorous assumptions on the spectrum distribution of background, which is not fully reasonable for the real collected hyperspectral data. Another fact is that because of the low spatial resolution of

978-1-5090-6454-0/17/$31.00© IEEE

hyperspectral images, a pixel may cover a large range of area which possesses rich surface materials. As a result, its spectrum signature is typically complex and may be a mixture of different components of ground objects. So typical statistic models are unable to simulate all the HSI pixels accurately.

Reed–Xiaoli (RX) is one of the most popular methods in statistical methods category. It was proposed by Reed and Yu. RX is recognized to be the benchmark method in many multispectral/hyperspectral detection applications [12-13]. In this method, a multivariate Gaussian model is assumed to characterize the local background pixels around the target. After estimating the mean vector and covariance matrix on the basis of the local neighborhood, the Mahalanobis distance between each examined pixel and the statistic model is calculated and compared with a threshold for the final discrimination. RX is modified up to now and some other methods appear [14-15], but the original assumption is statistical models. Gaussian and other similar statistical models may not be suitable for the real hyperspectral images. Moreover, the background statistics are susceptible to contamination of anomaly targets which will lead us to a high false alarm rate.

Other Anomaly Detection methods rely on the kernel theory which maps the original data into a higher dimensional feature space through a nonlinear mapping [16]. The greatest strength of kernel methods is that the discrimination between the target and the background can be enhanced in a high-dimensional feature space. Support vector data description (SVDD) [8, 14] is a nonparametric kernel-based anomaly detector, which can directly analyze the support region avoiding the prior assumption. SVDD supposes that the background is enveloped by a minimum enclosing hyper sphere in a high-dimensional feature space. Anomalies are identified as those who fall outside this hyper sphere. In many methods of this category, we must solve numerical equation. So, the kernel based methods suffer from the expensive computations even for a medium-sized hyperspectral image.

Covariance analysis is another strategy that can detect anomalies by similar specifications between adjacent pixels. Recent methods in this category is developed by the researchers [17-19]. More recently, Parzen Windowing (PW) has also been investigated in hyperspectral anomaly detection [13]. PW performs probability density function estimation in a window through a kernel function, without a specific assumption of the background distribution. Unfortunately, suffering from complex bandwidth selection, the PW-based anomaly detectors are computationally intensive as well.

Since HSI contains a large amount of spatial and spectral data, some methods employ feature selection/extraction [20] or image fusion [21-23]. In this paper, we use both spectral and spatial information for detecting anomalies instead of using only spectral information that was introduced in our previous work. We propose an anomaly detector without assuming background pdf or estimating its covariance matrix. Our proposed detector can adaptively estimate the background using the concept that each pixel in background can be approximately represented by its spatial neighborhoods, but anomalies cannot be made by adjacent pixels. Background pixels are constituted by l2-norm minimization of the representation weight vector. Distance-weighted regularization matrix is also used to adjust the contribution of each neighboring pixel in the optimization problem which simply can be solved in a closed-form manner. The proposed detector (CRBORAD) uses a sliding dual-window that surrounds each test pixel of HSI. The inner window serves as a guard band, whereas the outer window constitutes the background for the test pixel. Note that the dimension w_{in} of the sliding hollow window is selected according to the spatial resolution of the scene and the expected size of the anomaly targets and the dimension w_{out} of outer region should be large enough for estimating background without excessive contamination by other adjacent anomalies. Surrounding spatial neighborhoods within the dual-window are combined to produce a prediction for the test (central) pixel.

Although we endeavor to select window dimensions precisely, few pixels within the dual-window may be contaminated by noise, outlier or other adjacent anomalies in the image. Assuming these few outlier pixels produces errors for test (central) pixels prediction and background estimation. So, in the CRBORAD proposed method, we remove outlier pixels that significantly different from other dual-window within pixels based on a statistical theorem, and then we estimate background pixels. So that outliers cannot contaminate background approximation and it leads us to better accuracy for detecting anomalies in subsequent stages. In this way, background estimation can be achieved.

Once the background image is available, the residual image is constituted by subtracting the predicted background from the original HSI, and the anomalies can be determined in the residual image.

We propose Collaborative Representation-Based with Outlier Removal Anomaly Detector (CRBORAD) method for HSI Anomaly Detection, in this paper. The paper continues as follows. Section 2 presents steps of CRBORAD method and reviews main concepts related to CRBORAD, Section 3 shows the experimental results implemented on San Diego airport hyperspectral data and illustrates the superiority of the proposed method. Finally, conclusions appear in section 4.

II. CRBORAD METHOD

This section details the proposed CRBORAD for hyperspectral anomaly detection. In this method, the most significant component is the data analysis, without any *priori* assumption on the data distribution. We explain the CRBORAD method in algorithms: CRBORAD-DW in section A, then CRBORAD kernel versions in section B.

A. Collaborative-Representation-Based with outlier Removal Detector and Distance Weighted(CRBORAD-DW)

We can consider a 3D hyperspectral image in R^d by eqn.(1).

$$X = \{x_i\}_{i=1}^{n} \quad (1)$$

where n is the total number of pixels and x_i represents each pixel of the image. d is the number of spectral bands.

For each test pixel y (of size $d \times 1$), surrounding data are collected from sliding dual-window within pixels centered at the pixel y.

The selected pixels constitute a 2D matrix by eqn. (2).

$$\widetilde{X_s} = \{x_i\}_{i=1}^{s} \quad (2)$$

where x_i represents each pixel surrounded the test pixel. s is the number of surrounding dual-window within pixels and can be calculated by eqn. (3).

$$s = w_{out} \times w_{out} - w_{in} \times w_{in} \quad (3)$$

where w_{in} and w_{out} are inner and outer window sizes, respectively.

Now we remove outlier pixels that are significantly different from other dual-window within pixels, since few pixels within the dual-window may be contaminated by noise, outlier, or other adjacent anomalies in the image, errors for test (central) pixels prediction and background estimation are produced. In this way, outliers cannot contaminate background approximation and it leads us to better accuracy for detecting anomalies in subsequent stages. Based on a statistical theorem, we calculate mean and standard deviation of dual-window within pixels intensities and construct threshold values simply by eqn. (4) and eqn. (5).

$$threshold_{max} = \mu + 2 \times \sigma \quad (4)$$

$$threshold_{min} = \mu - 2 \times \sigma \quad (5)$$

where μ and σ are mean and standard deviation of dual-window within pixels intensities and $threshold_{max}$ and $threshold_{min}$represent maximum and minimum intensity thresholds. Pixels with intensity values greater than $threshold_{max}$ or smaller than $threshold_{min}$, are omitted in dual-window within pixels and are not considered in subsequent stages.

Therefore, the matrix X_s (of size $d \times s'$) is obtained for every test pixel y on its own local window. s' refers to the number of within pixels after outlier removal. Now, we want to find weight vector α such that y is determined by its neighborhood pixels in its local window. In other words, we want to minimize eqn. (6) under the constraint that $\|\alpha\|_2^2$ is minimized too. we use l2-norm minimization; because l1-norm minimization is not a general solution for all hyperspectral data.

$$\arg\min_{\alpha} \|y - X_s\alpha\|_2^2 \quad (6)$$

Combining these objectives, leads us to eqn. (7).

$$\arg\min_{\alpha} \|y - X_s\alpha\|_2^2 + \lambda \|\alpha\|_2^2 \quad (7)$$

where y is test pixel, X_s is matrix of outlier removed neighborhood pixels in the dual-window around pixel y. λ is a Lagrange multiplier for adjusting eqn. (7) in different 3D image backgrounds and α is weight vector that we want to find.

Eqn. (7) is equivalent to

$$\arg\min_{\alpha}[\alpha^T(X_s^T X_s + \lambda \mathrm{I})\alpha - 2\alpha^T X_s^T y] \quad (8)$$

For solving eqn. (8), we take derivation with regard to α and set the result equation to zero. In this way, α yields by eqn.(9).

$$\alpha = (X_s^T X_s + \lambda I)^{-1} X_s^T y \quad (9)$$

The parameter λ adjusts the norm of weight vectors in the image depending on its backgrounds. Some surrounding pixels may be quite similar to the center pixel and λ should allow them to have large coefficients in the representations. On the other hand, for those surrounding pixels that are quite different from the center pixel, the coefficients should be small. We also employ a distance-weighted Tikhonov regularization to control the weight vector that is introduced and used in [24-25], we apply this technique by using the following diagonal regularization matrix:

$$\tau_y = \begin{bmatrix} \|y - x_1\|_2 & \dots & 0 \\ \vdots & \ddots & \vdots \\ 0 & \dots & \|y - x_s\|_2 \end{bmatrix} \quad (10)$$

where x_1 x_2 $\dots$ x_s are the columns of X_s. Indeed, the Euclidean distances between the center pixel y to each of X_s pixels are calculated. Obviously, applying matrix τ_y can lead us to better results for anomaly detection; because nearer pixels are more important in the proposed collaborative representation method. So, the improved optimization problem becomes:

$$\arg\min_{\alpha} \|y - X_s\alpha\|_2^2 + \lambda \left\|\tau_y\alpha\right\|_2^2 \quad (11)$$

Following the same derivation, the solution to (11) becomes:

$$\alpha = (X_s^T X_s + \lambda\tau_y^T\tau_y)^{-1} X_s^T y \quad (12)$$

So α (of size $s' \times 1$) is obtained. Now we predict test pixel by reconstruction eqn. (13).

$$\hat{y} = X_s\alpha \quad (13)$$

where X_s is matrix of outlier removed neighborhood pixels in the dual-window around test pixel y and $\hat{y}$ is reconstructed test pixel.

Once the representation process is finished, residual image is obtained by directly subtracting the predicted background from the original hyperspectral data and anomalies can be determined in the residual image by eqn. (14).

$$r_1 = \|y - \hat{y}\|_2 = \|y - X_s\alpha\|_2 \quad (14)$$

If it is larger than a threshold, then y is declared as an anomalous pixel. The overall description of the CRBORAD-DW algorithm is given as Algorithm 1.

Algorithm 1 CRBORAD-DW Algorithm for Anomaly Detection

Input: Three-dimensional hyperspectral cube,
window size(w_{in} , w_{out}) and the regularization parameter λ

for all pixels **do**

1) For each test pixel y, a 2D matrix constitutes based on the dual-window within pixels by eqn. (2);
2) Removing outlier pixels that significantly are different from other within pixels and constructing the matrix X_s ;
3) Calculating the weight vector α by a closed-form of eqn. (12);
4) Calculating the distance measurement by eqn. (14) and comparing it with the prescribed threshold;

end for

Output: Anomaly detection map.

B. *Kernel Collaborative-Representation-Based with outlier Removal Detector(CRBORAD-Linear-Kernel, CRBORAD-Gaussian-Kernel)*

Kernel-based versions of feature extraction have recently been investigated in hyperspectral image analysis. Kernel-based methods can project the linearly nonseparable data into a feature space in which those data become more separable. Here, we extend the proposed CRBORAD into two kernel versions: Linear Kernal and Gaussian Kernel. The methods referred to as CRBORAD-Linear-Kernel and CRBORAD-Gaussian-Kernel.

In a kernel-induced feature space, after removing outliers and constituting matrix X_s ، the center pixel y **i**s represented by terms of kernel function by its surrounding data X_s. So, the new optimization problem becomes

$$\arg\min_{\alpha} \|\varphi(y) - \boldsymbol{\varphi}\alpha\|_2^2 + \lambda \left\|\tau_{\varphi(y)}\alpha\right\|_2^2 \quad (15)$$

where $\varphi(y)$ is the projected center pixel to the kernel-induced feature space by mapping function φ:

$$y \rightarrow \varphi(y) \in R^{D\times 1} \quad (16)$$

D is the dimension of kernel feature space, and $\boldsymbol{\varphi}$ is constructed by eqn. (17).

$$\boldsymbol{\varphi} = [\varphi(x_1), \varphi(x_2), \ldots., \varphi(x_{S'})] \in R^{D\times S'} \quad (17)$$

The new biasing Tikhonov matrix $\tau_{\varphi(y)}$then becomes:

$$\tau_{\varphi(y)} = \begin{bmatrix} \|\varphi(y) - \varphi(x_1)\|_2 & \ldots & 0 \\ \vdots & \ddots & \vdots \\ 0 & \ldots & \varphi(y) - \varphi(x_{S'}) \end{bmatrix} \quad (18)$$

$\tau_{\varphi(y)}$ elements are constructed by eqn. (19).

$$\|\varphi(y) - \varphi(x_i)\|_2 = [k(y,y) + k(x_i,x_i) - 2k(y,x_i)]^{1/2} \quad (19)$$

where $i = 1,2,\ldots.,S'$. After constituting $\tau_{\varphi(y)}$, the weight vector α (of size $s' \times 1$) is obtained by a closed-form solution of eqn. (20).

$$\alpha = (\boldsymbol{\varphi}^T\boldsymbol{\varphi} + \lambda\tau_{\varphi(y)}^T\tau_{\varphi(y)})^{-1}\boldsymbol{\varphi}^T\varphi(y) = (\boldsymbol{K} + \lambda\tau_{\varphi(y)}^T\tau_{\varphi(y)})^{-1}k(0,y) \quad (20)$$

Functions that are used in eqn. (20) are as follows:

$$k(0,y) = [k(x_1,y), k(x_2,y), \ldots. k(x_{s'},y)]^T \in R^{S'\times 1} \quad (21)$$

$$\boldsymbol{K} = \boldsymbol{\varphi}^T\boldsymbol{\varphi} \in R^{S'\times S'} \quad (22)$$

where $\boldsymbol{K}$ is Gram matrix kernel function with follow elements:

$$\boldsymbol{K}_{i,j} = k(x_i, x_j) \quad (23)$$

We use two commonly used kernel functions, Linear and Gaussian that referred to as CRBORAD-Linear-Kernel and CRBORAD-Gaussian-Kernel methods.

Linear function kernel is:

$$k(x_i, x_j) = \gamma {x_i}^T x_j (\gamma > 0) \quad (24)$$

and Gaussian radial basis function (RBF) kernel is

$$k(x_i, x_j) = \exp(-\gamma\|x_i - x_j\|_2^2)(\gamma > 0) \quad (25)$$

Then, the residual of the CRBORAD-Linear-Kernel and CRBORAD-Gaussian-Kernel are represented by eqn. (26).

$$r_2 = \|\varphi(y) - \boldsymbol{\varphi}\alpha\|_2 = \sqrt{(\varphi(y) - \boldsymbol{\varphi}\alpha)^T(\varphi(y) - \boldsymbol{\varphi}\alpha)} = \sqrt{k(y,y) + \alpha^T\boldsymbol{K}\alpha - 2\alpha^T k(0,y)} \quad (26)$$

III. Experimental Results

In order to evaluate the performance of the proposed CRBORAD method, it is implemented on San Diego airport hyperspectral data. The HSI images used herein are from the HYDICE push broom sensor with spectral sampling of 10 nm. It consists of 189 spectral bands with spatial resolution of 3.5 meters. We implement our method in 80×80 test region of this data. Band 19 of this data with its test region in RGB format and target map of anomalies in the test region are illustrated in Fig. 1. We implemented the proposed CRBORAD-DW, CRBORAD -Linear-Kernel and CRBORAD-Gaussian-Kernel algorithms using Matlab programs.

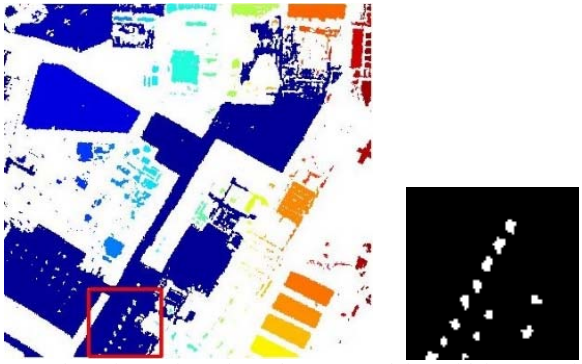

Fig. 1. Band 19 of San Diego airport hyperspectral data with its test region in RGB format and the target map

Tables 1-3 collect ROC's Area Under the Curve (AUC) values of the proposed CRBORAD method with different parameters. Fig. 2 illustrates ROC curves of CRBORAD-DW, CRBORAD-Linear-Kernel and CRBORAD-Gaussian-Kernel. As it was mentioned, we have three parameters for determining receiver operating characteristic (ROC) curve: dual window sizes: w_{in} , w_{out} and λ parameters. The effect of them is illustrated by AUC values in Tables 1-3. As we can see, λ=10 is the optimal value for our data. We select this λ value in Fig. 2 and we show ROC curves of the proposed CRBORAD method with varying window sizes.

Table 1. AUC values of the proposed CRBORAD-DW with different parameters for San Diego airport data

λ value	W_{in} \ W_{out}	9	11	13	15	17
10^0	5	0.9198	0.9204	0.9164	0.9104	0.9042
	7	0.9179	0.9198	0.9122	0.9098	0.9033
10^1	5	0.9202	**0.9204**	0.9164	0.9104	0.9056
	7	0.9187	0.9198	0.9122	0.9102	0.9052
10^2	5	0.9202	0.9204	0.9158	0.9104	0.9045
	7	0.9178	0.9196	0.9114	0.9102	0.9041
10^3	5	0.9201	0.9204	0.9148	0.9089	0.9038
	7	0.9174	0.9193	0.9114	0.9064	0.9040

Table 2. AUC values of the proposed CRBORAD-Linear-Kernel with different parameters for San Diego airport data

λ value	W_{in} \ W_{out}	9	11	13	15	17
10^0	5	0.9278	0.9287	0.9217	0.9156	0.9084
	7	0.9262	0.9272	0.9214	0.9082	0.9077
10^1	5	0.9278	**0.9287**	0.9223	0.9165	0.9087
	7	0.9265	0.9274	0.9214	0.9108	0.9082
10^2	5	0.9268	0.9287	0.9208	0.9147	0.9057
	7	0.9257	0.9268	0.9212	0.9062	0.9045

10^3	5	0.9264	0.9282	0.9187	0.9125	0.9022
	7	0.9252	0.9266	0.9207	0.9057	0.9018

Table 3. AUC values of the proposed CRBORAD-Gaussian-Kernel with different parameters for San Diego airport data

λ value	W_{in} \ W_{out}	9	11	13	15	17
10^0	5	0.9509	0.9518	0.9504	0.9467	0.9412
	7	0.9502	0.9509	0.9510	0.9462	0.9402
10^1	5	0.9512	**0.9527**	0.9514	0.9488	0.9417
	7	0.9509	0.9522	0.9509	0.9479	0.9405
10^2	5	0.9510	0.9517	0.9507	0.9468	0.9411
	7	0.9509	0.9510	0.9495	0.9466	0.9384
10^3	5	0.9502	0.9507	0.9487	0.9417	0.9517
	7	0.9495	0.9505	0.9465	0.9410	0.9365

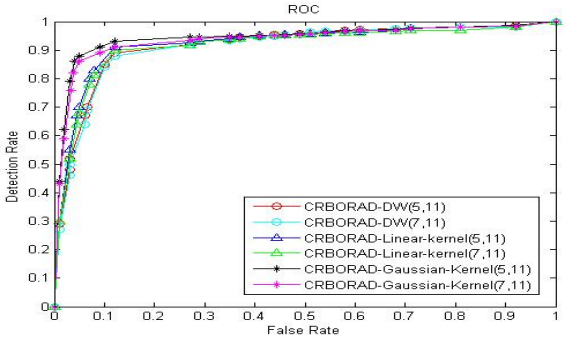

Fig. 2. ROC curves of CRBORAD method with varying window sizes

As we said later, λ is a Lagrange multiplier for adjusting equations in different 3D image backgrounds and regularizing the results dependent to data. For our data λ=10 is the optimal value. The dimension w_{in} of the sliding hollow window are selected according to the spatial resolution of the scene and the expected size of the anomaly targets, as we can see in the results, w_{in}=5 is an appropriate value for our data. The dimension w_{out} must be appropriate for estimating background. If w_{out} is too large the, adjacent dual-window within pixels may be contaminated by other adjacent anomalies and considering them as background is not true. So we must select an appropriate w_{out} value. We can see in AUC values of Tables 1-3, w_{out}=11 is the optimal appropriate value for our data.

ROC curves of Fig. 2 shows better accuracy of CRBORAD-Gaussian-Kernel respect to CRBORAD-Linear-Kernel and CRBORAD-DW methods. Indeed, mathematical Gaussian equations of CRBORAD-Gaussian-Kernel is more precise for determining background central pixels than mathematical Linear equations in CRBORAD-Linear-Kernel and CRBORAD-DW methods.

As we can see, CRBORAD-Gaussian-Kernel is the most precise method in our proposed CRBORAD methods. So, we compare CRBORAD-Gaussian-Kernel with other previous methods. Four HSI Anomaly Detection algorithms are used for comparison to proposed CRBORAD-Gaussian-Kernel method: RX, PCA and other two new methods: CRD-DW-STO [17] and kernel-CRD [17]. For more intuitive sensing of outputs, target map and anomaly map of each method are illustrated in Fig. 3; and Fig. 4 illustrates the performance of CRBORAD-Gaussian-Kernel versus RX, PCA and other two new methods: CRD-DW-STO and kernel-CRD for San Diego airport hyperspectral data by receiver operating characteristic (ROC) curves. We can see CRBORAD-Gaussian-Kernel noticeably outperforms RX method and provides better performance to PCA, CRD-DW-STO and kernel-CRD.

As it was mentioned above, few pixels within the dual-window may be contaminated by noise, outlier or other adjacent anomalies in the image that produces errors for the test (central) pixels prediction and background estimation. Considering a fixed λ value in CRD-DW-STO and kernel-CRD methods is not precise for covering these positions in homogeneous and heterogeneous backgrounds, accurately.

If the central pixel y is a normal pixel and few adjacent dual-window within pixels are anomalous, the corresponding intensity values of the anomalous pixels reflect on the diagonal regularization matrixτ_y . As a result, it causes the approximation of $\hat{y}$ to be different from $\mathbf{the}$ test (central) pixel. So, in the residual image, the normal central pixel may be declared as anomalous by CRD-DW-STO and kernel-CRD algorithms. In this way, background information is declared as anomalous and False Rate (FR) increased. On the other hand, If the central pixel y is an anomalous pixel and few adjacent dual-window within pixels are anomalous too, the corresponding intensity values of the anomalous adjacent pixels reflect on the diagonal regularization matrix τ_y . As a result, it causes the approximation of $\hat{y}$ to be close to $\mathbf{the}$ test (central) pixel. So, in the residual image, the anomalous central pixel may not be declared as anomalous by CRD-DW-STO and kernel-CRD algorithms. In this way, some anomalies are not declared and Detection Rate (DR) decreased. Outlier removal from adjacent dual-window pixels based on a statistical theorem, before applying the main algorithm, is an appropriate solution for these non-desirable positions. Fig. 3. and Fig. 4 illustrate more precise results of CRBORAD-Gaussian-Kernel method versus other previous methods.

Table 4. presents each ROC's area under the curve (AUC) along with computation time for anomaly detection. AUC value is improved in CRBORAD-Gaussian-Kernel respect to other methods. It means that CRBORAD-Gaussian-Kernel leads us to better accuracy for detecting anomalies.

Execution time of CRBORAD-Gaussian-Kernel decreases respect to kernel-CRD, but it increases respect to RX, PCA and CRD-DW-STO methods. To measure the execution time, we use a personal computer with Microsoft 8 OS, core™ i7-4500U, CPU @1.8GHz 2.4GHz and 8 GB RAM. The codes are run by MATLAB® 2014a. It is obvious that the implementation of the proposed algorithms using a C compiler and employing a GPU based parallel processing architecture increases the execution speed for real time applications. However greater AUC (Area Under Curve) value, proves the superiority of the proposed CRBORAD-Gaussian-Kernel method.


(a)


(b)

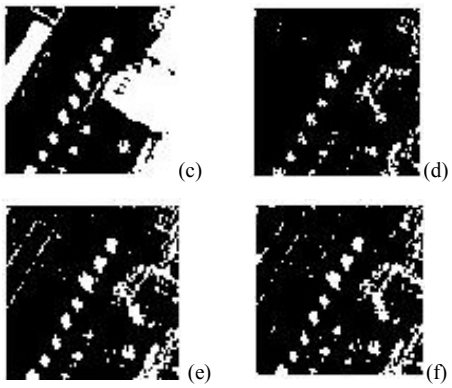

Fig. 3. (a) Target map and Anomaly map of (b) RX, (c) PCA, (d) CRD-DW-STO, (e) kernel-CRD and (f) CRBORAD-Gaussian-kernel

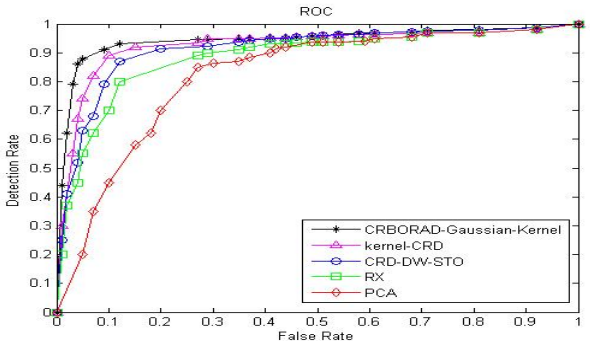

Fig. 4. ROC curves: performance of CRBORAD-Gaussian-Kernel comparing with RX, PCA, CRD-DW-STO and kernel-CRD

Table 4. ROC's Area Under the Curve (AUC) values and execution times

Method	CRBORAD-Gaussian-Kernel	kernel-CRD [17]	CRD-DW-STO [17]	PCA	RX
AUC	0.9527	0.9305	0.9104	0.7829	0.8667
Runtime(sec)	112.6406	158.125	22.0312	56. 8906	15.0156

IV. CONCLUSION

An accurate and efficient algorithm based on pixels collaborative representation of pixels for anomaly detection is presented. In this algorithm, after removing outlier pixels that are significantly different from adjacent majority of pixels, within a sliding dual window, background pixels are estimated. We used a linear combination of surrounding samples based on the distance weighted and **Kernel extensions of the proposed approach. Then** the residual image is constituted by subtracting the predicted background from the original HSI; So anomalies are detected. We implemented the proposed CRBORAD algorithm on San Diego airport hyperspectral data. Comparing the results with four popular and previous methods, confirms the superiority of the proposed method.

REFERENCES

[1] L. Zhang, D. Tao, X. Huang, B. Du, and L. Zhang, "Hyperspectral remote sensing image subpixel target detection based on supervised metric learning," *IEEE Trans. Geosci. Remote Sens.*, vol. 52, no. 8, pp. 4955–4965, Aug. 2014.

[2] L. Zhang, L. Zhang, D. Tao, X. Huang, and B. Du, "Compression of hyperspectral remote sensing images by tensor approach" *Neurocomputing*, vol. 147, pp. 358–363, Jan. 2015.

[3] J. Theiler and B. Wohlberg, "Local coregistration adjustment for anomalous change detection," *IEEE Trans. Geosci. Remote Sens.*, vol. 50, no. 8, pp. 3107–3116, Aug. 2012.

[4] B. Luo, C. Yang, J. Chanussot, and L. Zhang, "Crop yield estimation based on unsupervised linear unmixing of multidate hyperspectral imagery,"*IEEE Trans. Geosci. Remote Sens.*, vol. 51, no. 1, pp. 162–173, Jan. 2013.

[5] H. Ghassemian, "A retina based multi-resolution image fusion", International Geoscience and Remote Sensing Symposium (IGARSS), 2, pp. 709-711, 2001.

[6] S. Matteoli, N. Acito, M. Diani, and G. Corsini, "An automatic approach to adaptive local background estimation and suppression in hyperspectral target detection," *IEEE Trans. Geosci. Remote Sens.*, vol. 49, no. 2, pp. 790–800, Feb. 2011.

[7] G. Yanfeng, L.Ying, etal, "A Selective KPCA algorithm based on high- order statistics for anomaly detection in hyperspectral imagery", IEEE Geosci. Remote Sens. Lett.5(1)(2008)43–47.

[8] P. Gurram, H. Kwon, and T. Han, "Sparse kernel-based hyperspectral anomaly detection," *IEEE Geosci. Remote Sens. Lett*, vol. 9, no. 5, pp. 943–947, Sep. 2012.

[9] S. Matteoli, M. Diani, and J. Theiler, "An overview of background modeling for detection of targets and anomalies in hyperspectral remotely sensed imagery," *IEEE J. Sel. Topics Appl. Earth Observ. Remote Sens.*, vol. 7, no. 6, pp. 2317–2336, Jun. 2014.

[10] S. Khazai, A. Safari, B. Mojaradi, and S. Homayouni, "An approach for subpixel anomaly detection in hyperspectral images," *IEEE J. Sel. Topics Appl. Earth Observ. Remote Sens.*, vol. 6, no. 2, pp. 769–778, Apr. 2013.

[11] B. Du and L. Zhang, "A discriminative metric learning based anomaly detection method," *IEEE Trans. Geosci. Remote Sens.*, vol. 52, no. 11, pp. 6844–6857, Nov. 2014.

[12] B. Du and L. Zhang, "Random-selection-based anomaly detector for hyperspectral imagery," *IEEE Trans. Geosci. Remote Sens.*, vol. 49, no.5, pp. 1578–1589, May 2011.

[13] S. Matteoli, T. Veracini, M. Diani, and G. Corsini, "Models and methods for automated background density estimation in hyperspectral anomaly detection," *IEEE Trans. Geosci. Remote Sens.*, vol. 51, no. 5, pp. 2837–2852, May 2013.

[14] S. Khazai, S. Homayouni, A. Safari, and B.Mojaradi, "Anomaly detection in hyperspectral images based on an adaptive support vector method," *IEEE Geosci. Remote Sens. Lett*, vol. 8, no. 4, pp. 646–650, Jul. 2011.

[15] B. Du, R. Zhao, L. Zhang, "A spectral-spatial based local summation anomaly detection method for hyperspectral images", Signal Processing, Vol. 124, pp. 115–131, , July 2016.

[16] M. Borhani and H. Ghassemian, "Kernel Multivariate Spectral-Spatial Analysis of Hyperspectral Data," Selected Topics in Applied Earth Observations and Remote Sensing, IEEE Journal of, vol. 8, pp. 2418-2426, 2015.

[17] W. Li and Q. Du, "Collaborative Representation for Hyperspectral Anomaly Detection", *IEEE Trans. Geosci. Remote Sens.*, Vol. 53, No. 3, March 2015.

[18] Y. Yuan, Q. Wang, and G. Zhu, "Fast hyperspectral anomaly detection via high-order 2-D crossing filter," *IEEE Trans. Geosci. Remote Sens.*, vol. 53, no. 2, pp. 620–630, Feb. 2015.

[19] A. Taghipour, H. Ghassemian and F. Mirzapour, "Anomaly Detection of Hyperspectral Imagery Using Differential Morphological Profile", 24th Iranian Conference on Electrical Engineering (ICEE), Shiraz, Iran, 10-12 May 2016.

[20] M. Imani and H. Ghassemian,. "Feature extraction using attraction points for classification of hyperspectral images in a small sample size situation", *IEEE Trans. Geosci. Remote Sens.*, 11 (11), 6809181, pp. 1986-1990, 2014.

[21] M. Ghahremani and H. Ghassemian, "Remote sensing image fusion using ripplet transform and compressed sensing", *IEEE Trans. Geosci. Remote Sens.*, 12 (3), 6883128, pp. 502-506, 2015.

[22] F. Mirzapour and H. Ghassemian, "Improving hyperspectral image classification by combining spectral, texture, and shape features",

International Journal of Remote Sensing, 36(4), pp. 1070-1096, 2015.
[23] H.R. Shahdoosti and H. Ghassemian, "Fusion of MS and PAN images preserving spectral quality", *IEEE Trans. Geosci. Remote Sens.*, 12 (3), 2353135, pp. 611-615, 2015.
[24] W. Li and Q. Du, "Unsupervised nearest regularized subspace for anomaly detection in hyperspectral imagery", in Proc. IEEE Int. Geosci. Remote Sens. Sym. Melbourne, Vic., Australia, pp. 1055–1058, Jul. 2013.
[25] W. Li, E. W. Tramel, S. Prasad, and J. E. Fowler, "Nearest regularized subspace for hyperspectral classification", IEEE Trans. Geosci. Remote Sens., vol. 52, no. 1, pp. 477–489, Jan. 2014.